Physics – Uspekhi **57** (9) 877 – 890 (2014)

FROM THE CURRENT LITERATURE PACS numbers: **28.52. – s**, 47.40.Nm, 52.50.Lp

On thermonuclear processes in cavitation bubbles

R I Nigmatulin, R T Lahey, Jr., R P Taleyarkhan, C D West, R C Block

DOI: 10.3367/UFNe.0184.201409b.0947

Contents

Abstract. The theoretical and experimental foundations of so-called bubble nuclear fusion are reviewed. In the nuclear fusion process, a spherical cavitation cluster $\sim 10^{-2}$ m in diameter is produced of spherical bubbles at the center of a cylindrical chamber filled with deuterated acetone using a focused acoustic field having a resonant frequency of about 20 kHz. The acoustically-forced bubbles effectuate volume oscillations with sharp collapses during the compression stage. At the final stages of collapse, the bubble cluster emits 2.5 MeV D – D fusion neutron pulses at a rate of ~ 2000 per second. The neutron yield is $\sim 10^5$ s^{-1}. In parallel, tritium nuclei are produced at the same yield. It is shown numerically that, for bubbles having sufficient molecular mass, spherical shock waves develop in the center of the cluster and that these spherical shock waves (microshocks) produce converging shocks within the interior bubbles, which focus energy on the centers of the bubbles. When these shock waves reflect from the centers of the bubbles, extreme conditions of temperature ($\sim 10^8$ K) and density ($\sim 10^4$ kg m^{-3}) arise in a (nano)spherical region ($\sim 10^{-7}$ m in size) that last for $\sim 10^{-12}$ s, during which time about ten D – D fusion neutrons and tritium nuclei are produced in the region. A paradoxical result in our experiments is that it is bubble cluster (not streamer) cavitation and the sufficiently high molecular mass of (and hence the low sound speed in) D-acetone (C_3D_6O) vapor (as compared, for example, to deuterated water D_2O) which are necessary conditions for the formation of convergent spherical microshock waves in central cluster bubbles. It is these waves that allow the energy to be sufficiently focused in the nanospherical regions near the bubble centers for fusion events to occur. The criticism to which the concept of 'bubble fusion' has been subjected in the literature, in particular, most recently in *Uspekhi Fizicheskikh Nauk* (*Physics – Uspekhi*) journal, is discussed.

R I Nigmatulin P P Shirshov Institute of Oceanology, Russian Academy of Sciences, Nakhimovskii prosp. 36, 117997 Moscow, Russian Federation
E-mail: nigmar@ocean.ru
R T Lahey, Jr., R C Block Rensselaer Polytechnic Institute, 110 8th Street, Troy, New York 12180-3590, USA
E-mail: laheyr@rpi.edu, blockr@rpi.edu
R P Taleyarkhan Purdue University, 400 Central Drive, W. Lafaette, IN 47907-1290, USA
E-mail: rusi@purdue.edu
C D West 242 Joel Road, Oliver Springs, TN 37840, USA
E-mail: herderwest@comcast.net

Received 30 December 2013, revised 24 March 2014
Uspekhi Fizicheskikh Nauk **184** (9) 947 – 960 (2014)
DOI: 10.3367/UFNr.0184.201409b.0947
Translated by the authors; edited by A Radzig

1. Introduction

The focusing (i.e., cumulation) of energy by the spherically symmetrical convergent flow of an inviscid and incompressible fluid around a spherical cavity (bubble), when the pressure in it is constant, notably zero, is described by the famous Rayleigh equation. E I Zababakhin (see monographs [1] and [2]) showed the influence of the viscosity and compressibility of the external fluid, which lowers the intensity of cumulation. However, if the driving pressure difference between that far away from the bubble and that in the bubble is large enough, they do not prevent an unlimited value of pressure in some zone close to the bubble interface (see also the well-known book by Ya B Zel'dovich and Yu P Raizer [3]). The limitation on the pressure rise is caused, first, by the gas (vapor) that always fills the bubble and brakes the convergent fluid and, second, by growing disturbances of the spherically symmetrical convergent flow and bubble distortion/break-up.

The strong compressibility of a substance needed for the realization of nuclear reactions by spherically symmetrical shock compression (i.e., implosion) of a spherical volume with a diameter of ~ 1 m was extensively analyzed during the development of nuclear weapons. Later on, in the 1990s, such focusing of kinetic energy attracted attention in connection with paradoxes encountered in numerous experiments on bubble sonoluminescence [3–6]. In these experiments, tiny bubbles measuring about 10 μm in diameter were subjected to periodic compression and expansion using an acoustic field. At the end of implosive compression stage, very sharp compression occurred, and the diameter of the bubbles very quickly diminished to less than 1 μm. At this moment,

intensive light pulses of very short duration, sometimes only 50 ps, were emitted.

Experimental investigations and numerical calculations have shown that the temperature in the center of a bubble filled with air or nitrogen may reach $T_* \sim 10^6$ K. In connection with these estimations, the possibility of D + D thermonuclear fusion in a bubble filled with deuterium gas, D_2, or the vapor of heavy water, D_2O, was postulated. It is important to note that an almost adiabatic bulk compression of all the mass of the gas/vapor in the bubble can only produce a temperature on the order of 5000 K. Nevertheless, the high temperatures produced by shock wave cumulation (focusing) of energy near the center of the bubble explain why ultrashort sonoluminescent light flashes may be observed [4–6].

Figure 1 depicts a schematic of the supercompression process. The sphere of radius $R(t)$ corresponds to the bubble interface. When the interface ('piston') reaches a large enough velocity toward the center of the bubble, a converging spherical shock, a wave of radius $r_f(t)$ (Fig. 1b), is initiated. Due to the focusing of the shock wave and its reflection from the bubble's center, a tiny spherical volume of radius r_* is generated (Fig. 1c), having a completely ionized gas (plasma). This plasma has an extremely high temperature and density over a very short time interval t_*. Hydrocode calculations [7] have shown[1] that the plasma in a tiny spherical volume ($r < r_* \sim 3$ μm) during a time interval of $t_* \sim 50$ ps has a temperature $T > 10^5$ K and density $\rho \sim 10^4$ kg m^{-3}, and during a still shorter time interval of $t_{**} \sim 1$ ps the local temperature of the plasma may reach $T > 10^6$ K. It is also shown in Ref. [7] that the maximum temperature for a bubble having an initial size of ~ 10 μm and filled with deuterium (D_2) gas or heavy water (D_2O) vapor is less than for a bubble filled with air or nitrogen, and thus under these conditions thermonuclear reactions cannot be realized. Hence, the authors of Ref. [7] concluded that D + D thermonuclear fusion cannot occur in sonoluminescence type experiments.

Nevertheless, the authors of the present paper decided to explore how we can amplify the cumulation process in bubbles compared with that in sonoluminescence experiments, using other regime parameters of the process. First, other parameters of bubbly liquids which determine the sizes of the bubble and their content can be chosen. Second, it is necessary to use a different experimental technique and obtain a more intensive acoustic field.

The fact that thermonuclear reactions can take place within collapsing vapor bubbles (a process called 'bubble fusion') has been discussed in detail in a number of peer-reviewed archival publications [8–19], which represent over a decade of bubble fusion research findings. A detailed description in Russian was also presented in a small circulation edition [13]. Anyway, the original publication concerning the experimental realization of bubble fusion followed extensive debates and reviews in 2001 at the Oak Ridge National Laboratory (ORNL), where our first experiments were conducted. As a consequence of those discussions and reviews, ORNL management authorized the publication of our experimental results. The seminal publication appeared in *Science* [10] after this paper was subjected to a very stringent peer review process by this prestigious scientific journal. Given the potential scientific importance of this work, it was accompanied by a special editorial from Dr. Kennedy, Editor-in-Chief of *Science* [10], who wrote about the controversy surrounding our discovery, including calls and letters from those who, without any real scientific arguments, simply did not want our paper to be published.

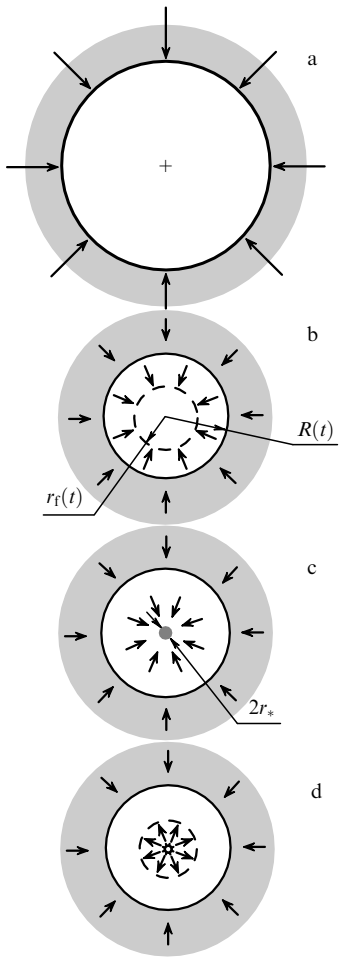

Figure 1. Schematic of bubble compression: (a) initial compression; (b) shock wave formation: $r_f(t)$ is the front of the shock wave, and $R(t)$ is the radius of the bubble; (c) stage with extreme compressed plasma in the central zone (with radius r_*) of the bubble, where thermonuclear reactions may occur, and (d) stage of expansion of the extreme zone.

After our *Science* paper appeared, our bubble fusion results were presented and discussed at numerous technical conferences and seminars on nuclear physics, explosion physics, acoustics, and fluid dynamics. Nevertheless, a group of determined opponents to our discovery decided to use journalists to discredit our findings instead of engaging in scientific discussions. For example, *Nature News* published a number of articles written by journalist E Reich [22], who wrote on various topics, which were highly critical of the lead author (Dr. Taleyarkhan[2]) without mentioning us, his coauthors, and with a total refusal to present alternative

[1] We note that in Ref. [7] heat and mass exchange were taken into account incorrectly (see Refs [8, 9]) during the expansion stage and the initial stage of compression of the bubble. In a bubble ~ 10 μm in size during expansion or compression, the temperature of the gas has time to follow the constant temperature of the liquid (i.e., the process in the gas is isothermal rather than adiabatic, as was assumed in work [7]). Moreover, vapor from interfacial evaporation and condensation must also be taken into account. All these corrections influenced the estimates for r_*, t_*, and T_*.

[2] This name was added in the English proof.

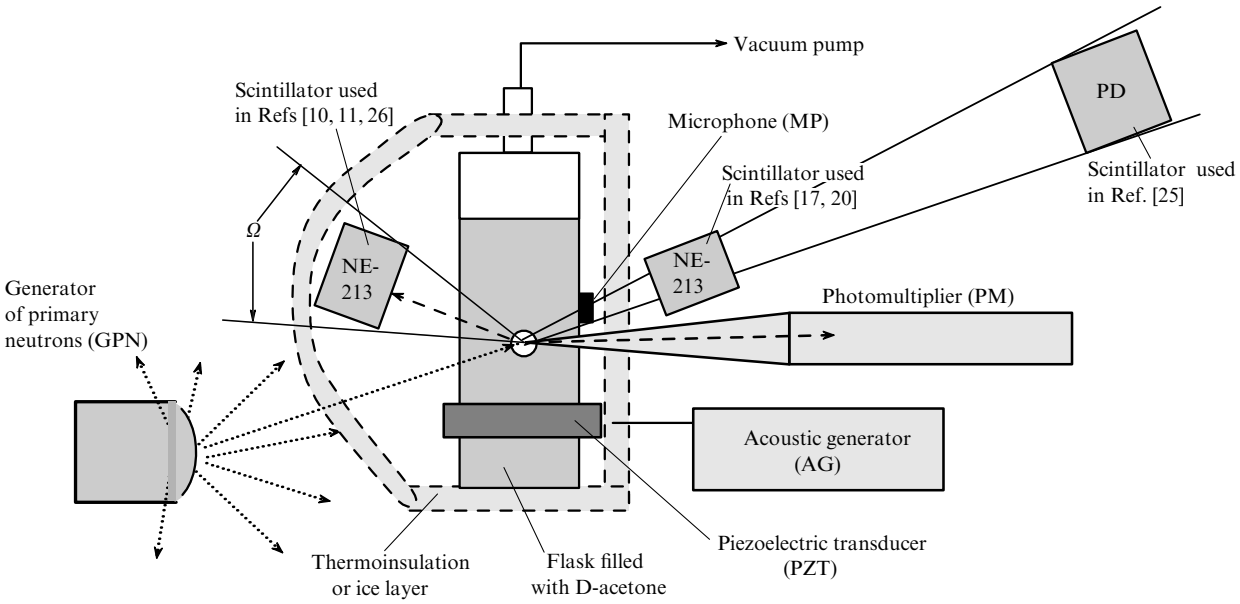

Figure 2. A schematic of the bubble fusion experiments [10–11, 17, 20, 26].

points of view. Also, in the USA a congressman was persuaded by some of our detractors to suggest that this author may have falsified these experimental results. As a consequence, several independent scientific commissions, one after another, examined the accusations and dismissed all of them as baseless attacks on the quality, performance, and accuracy of our bubble fusion experiments. Nevertheless, still another review group found a reason to accuse Dr. Taleyarkhan of 'research misconduct', which consisted of the fact that he encouraged the inclusion as a coauthor of paper [20] of an undergraduate student whose contribution seemed to be insignificant. Because of these investigations and charges (none of which showed that anything was wrong with our bubble fusion results nor those of separate confirmatory studies by two other teams [20, 26]), the preconceived opinions of many in the scientific community concerning bubble fusion became negative, which chilled further research in this area of technology.

This whole dreary story of problems has been carefully documented by S Krivit in *New Energy Times* [23].

The process of gas and vapor bubble collapse is attended by a whole number of paradoxes, and it has potential for nuclear technologies. Recently, *Physics–Uspekhi* broke the period of doubt, formulated and published largely outside the scientific community, by publishing a letter to the Editors by Goverdovskii, Imshennik, and Smirnov [24]. The authors of this article criticized the neutron and tritium measurements made by us at Oak Ridge National Laboratory and presented in our publications [10–12], as well as the separate bubble fusion experiments carried out by Xu and Butt [20] at Purdue University. In addition, they concluded on the basis of a rather primitive theoretical scheme that it is fundamentally impossible to achieve the conditions needed for significant nuclear fusion in an imploding vapor bubble.

It should be noted that similar critical statements were considered and refuted more than once at seminars and in the responses to reviewers of our papers. Nevertheless, negative prejudices linger on, as evidenced by our critics repeating their arguments but never commenting on our responses to their criticism. Clearly, a careful scientific analysis of the interesting and paradoxical physical phenomena which occur during implosive vapor bubble collapse and the possibility of bubble fusion, which has something in common with laser fusion, are relevant. The analysis presented below takes into account the arguments of all our critics, past and present, and shows them to be baseless.

2. Analysis of experiments

The publications in question [10–20] deal with experiments (Fig. 2) in which a cylindrical glass test chamber (6.5 cm in diameter and 20 cm high) was filled with chilled (about 0 °C), deuterated, and degassed acetone (C_3D_6O), and contained an induced approximately spherical bubble cluster (~ 1 cm in diameter) of relatively small vapor-filled cavitation bubbles, each having a maximum diameter of about 0.5 to 0.8 mm. Use was made of an acoustic generator (AG) and a piezoelectric transducer (PZT) formed into a cylindrical ring and mounted on the outer surface of a cylindrical Pyrex glass chamber. The AG produced an approximately spherical acoustic pressure field at one of the resonant acoustic frequencies ($f_{ac} \approx 19.3$ kHz) of the D-acetone-filled test chamber, which corresponds to an acoustic cycle period of $f_{ac}^{-1} \approx 52$ μs.

An external source for generating primary neutrons (GPN) was used for the creation of a cavitation-induced bubble cluster. Usually, it was an accelerator-driven pulsed neutron generator (PNG) emitting monoenergetic 14.1-MeV neutrons at a rate of $Q_1 \approx 5 \times 10^5$ n/s at a repetition rate of $f_1 \approx 200$ Hz. In experiments conducted by another team [20], a Pu–Be continuously random isotopic neutron source delivering an intensity of $Q_1 \sim 2 \times 10^6$ n/s (at energies up to 10 MeV) was used. Also, in order to avoid any external neutron background concerns, instead of using external neutrons to nucleate bubble clusters, the recoils from alpha decays from a dissolved uranium salt were used in separate self-nucleation experiments [17].

During GPN-nucleated experiments, the neutron emission rates were measured utilizing a carefully calibrated 5 cm × 5 cm NE-213 liquid scintillator detector system.

Sonoluminescence light emissions were also detected using a photomultiplier (PM), and shocks on the flask wall were detected making use of surface-mounted microphones (MPs). In addition, tritium concentration changes in samples of the acetone were measured with the aid of a Beckman liquid scintillator spectrometer [10–12].

For self-nucleated experiments [17] with cavitation by alpha-particles, besides the NE-213 scintillator, three independent neutron-gamma detectors were applied: an LiI detector, multiple (passive) CR-39 track-edge detectors, and an NaI scintillation detector.

In most of the experiments, test chamber cooling was accomplished by housing the whole experimental setup in a refrigerated enclosure. However, the flask was surrounded in some experiments either by a plastic insulating sheet or ice packs. Also, in Fig. 2 it is shown that in some experiments [17, 20] and measurements [25] the NE-213 scintillation detectors were shielded from the test chamber by thermal insulation and ice packs, while in other experiments [10, 11, 26] the scintillators were not shielded.

In the present paper, eight modes of the experiments performed with the operation of the GPN and AG are discussed. They are distinguished by three two-valued characteristics:

(1) with bubble cluster cavitation or without cavitation (by using an AG frequency-phase shift approach);

(2) with either D-acetone/D-benzene or H-acetone/H-benzene in the acoustic chamber;

(3) with the liquid pool cooled to 0 °C or at room temperature (20 °C).

There were four modes with cluster cavitation and four without cavitation.

Under the action of an induced ultrasonic pressure field, which had a frequency of approximately 20 kHz (or, more precisely, 19.3 kHz), the bubbles in the cluster underwent volumetric oscillations with a sharp/implosive collapse at the end of the compression stage. At the moment of their maximum compression, when their radius decreased (by our estimation) to about 20 μm, the bubbles emitted strong divergent acoustic waves, which were detected by microphones on the external wall of the flask (see Fig. 2), and short SL light flashes were also detected. Significantly, for one and only one of these eight modes, namely

(1) with bubble cluster cavitation in chilled fluids,

(2) with D-acetone/D-benzene,

(3) with continuous test cell liquid pool cooling (~ 0 °C),

scintillations due to secondary neutron emissions occurred with an energy of 2.5 MeV. These neutron signals were time correlated with the sonoluminescence (SL) light flashes registered by the PM, and the shocks on the flask wall registered by the MP. At the same time, an accumulation of tritium occurred in the chilled D-acetone pool.

Measurement of 2.5-MeV fast neutrons and the corresponding tritium accumulation showed that D + D thermonuclear fusion had occurred [10].

In the external PNG neutron-induced tests, according to our measurements [10, 11] and the measurements taken by another team [20], the frequency f_2 of the neutron pulses and neutron productivity Q_2 were respectively equal to

$$f_2 = (2.3 \pm 0.2) \times 10^3 \text{ s}^{-1}\,, \qquad Q_2 = (4 \pm 1) \times 10^5 \text{ n/s}\,. \tag{2.1}$$

This means that $Q_2/f_2 \sim 150-200$ neutrons were in each pulse. At the same time, the generation of tritium nuclei occurred with the same productivity [12].

In self-nucleation experiments in which the bubble cluster nucleation was initiated by alpha-recoil particles from a dissolved uranium salt [17, 26], the cavitation bubble cloud formation rate was lower (~ 5 per second versus 40 per second), and, as expected, the D + D neutron emission rate was also lower, namely

$$Q_2 \sim 10^4 \text{ n/s}\,. \tag{2.2}$$

At room temperature (≈ 20 °C) in D-acetone, no experiments ever indicated neutron or tritium production. Our numerical simulations [9] showed that a much larger mass of vapor is evaporated in the cavitating bubbles at the higher liquid pool temperature; thus, for a fixed AG power, this larger mass of vapor weakened the supercompression effects.

The D + D fusion neutron emission rate Q_2 was measured as the difference ΔN_2 in the number of scintillations N_c during a fixed time interval Δt ($\Delta t \sim 300$ s) of operation with bubble cluster cavitation minus the number of scintillations N_1 during the same time interval Δt of operation without bubble cluster cavitation:

$$Q_2 = \frac{\Delta N_2}{\eta_2 \Delta t} \qquad (\Delta N_2 = N_c - N_1)\,, \tag{2.3}$$

where η_2 is the net efficiency of our neutron detection system. Notice that N_1 includes the number of background scintillations due to the external neutrons arrived from the GPN. A typical intensity was $N_1/\Delta t \sim 500$ n/s.

Later on, Xu and Butt [20] showed that after executing about $n \approx 50$ acoustic oscillations a bubble cluster loses its spherical shape and eventually disappears; therefore, the D + D fusion neutron emissions also terminate. A new generation of secondary neutrons commenced after the formation of a new spherical cluster [11]. Taking into account the frequency f_2 of neutron pulses [see Eqn (2.1)], we arrive at a bubble cluster formation frequency $f_{cl} \approx f_2/n \sim 40-50 \text{ s}^{-1}$.

If bubble cavitation takes place as bubbly streamers (Fig. 3b), rather than clusters, then there was never any secondary neutron generation ($\Delta N_2 = 0$) because of the absence of bubble cluster focusing of the acoustic pressure waves [9, 16]. This is very important, and it should be noted that an experimentalist needs some experience for nucleating good bubble clusters.

Moreover, the increment ΔN_2 [see formula (2.3)] in the registered number of scintillations having energy E that varies within the range

$$0.7 < E < 2.45 \text{ MeV} \tag{2.4}$$

in the flask with chilled D-acetone was given by

$$\Delta N_2 = \chi N_1\,. \tag{2.5}$$

One has to bear in mind that GPN productivity was fixed: $Q_1 \approx 5 \times 10^5$ n/s, and for the conditions of the ORNL experiments [10] we got

$$\chi = 0.04\,. \tag{2.5a}$$

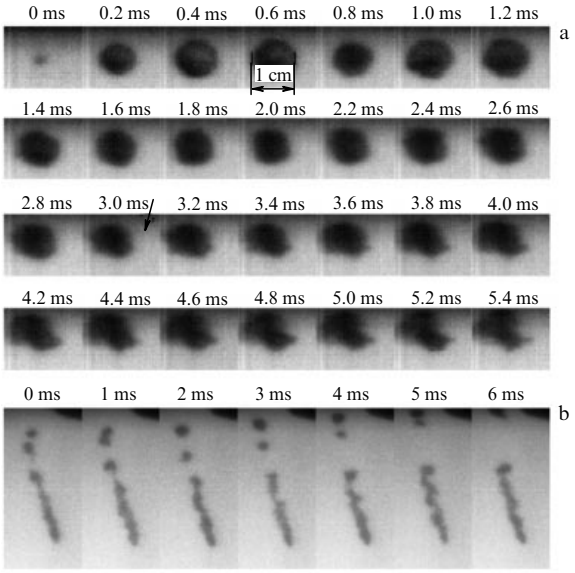

Figure 3. Photographs of bubble cluster (a) and streamer (b) regimes of cavitation. In the fourth picture from the left in the upper row, the diameter of the bubble cluster is shown (≈ 1 cm).

In contrast, in other experiments [11], which used more efficient setups for bubble cluster cavitation and detection of the primary and the secondary neutrons, we got

$$\chi = 0.35 \pm 0.2\,. \tag{2.5b}$$

So, the number of scintillations specified by the secondary (thermonuclear) neutrons compared with the background number of scintillations, N_1, generated by the primary neutrons from GPN, is a measurable and statistically significant value.

One should also remember that an increase in the number of registered scintillations takes place only for one experimental regime: bubble cluster cavitation in chilled D-acetone. For the other cavitation regimes (i.e., with room temperature D-acetone and with cooled or noncooled H-acetone), the increment of nuclear scintillations due to cluster and noncluster cavitation was statistically insignificant:

$$\chi = \pm 0.9 \times 10^{-2}\,. \tag{2.6}$$

It is also important to note that for all cavitational regimes there was never a statistically significant growth of the incremental neutron scintillations, ΔN_2, having energies greater than those associated with D–D fusion, i.e.

$$E > 2.5\ \text{MeV}\,, \tag{2.7}$$

though the number N_1 of background signals from the primary neutrons emitted by the PNG were quite numerous. A few counts did appear in higher energy channels due to pulse pile-up, smearing of the proton recoil edge, and some gamma photons leaking through the pulse shape discrimination process.[3]

[3] This sentence was added in the English proof.

3. Analysis of some critical remarks on the experiments

Goverdovskii et al. [24] offer their own estimates of D + D fusion-induced neutron emission and tritium production rates from our group's bubble fusion experiments, which utilized chilled D-acetone with PNG-induced cavitation. Our response herein corrects several factual errors and oversights in their conclusions and analyses.

By mistakenly assuming that the efficiency of our NE-213 neutron detector system was $\eta_s = 0.1$, while actually it was a much smaller value, Goverdovskii et al. [24] allege that our published productivity of fusion neutrons, Q_2, was greatly overestimated. For elucidation, we have to recount elements of the theory of neutron measurements. Our critics should have known that $\eta_s = 0.1$ is only the *intrinsic* efficiency of the scintillator-based system itself, when used in a largely gamma photon-free background. To calculate the overall net efficiency of the *system* involved for detecting neutrons that originated from a bubble cluster in our acoustic test chamber, we must not only consider our detector's intrinsic efficiency η_s, but also take into account three other important factors [27, 28].

(1) The solid angle, subtended by the scintillator, relative to the spherically symmetric source of neutrons, which is given by

$$\Omega \approx \frac{s}{4\pi L^2} = \frac{a^2}{4L^2}\,, \tag{3.1}$$

where $s = \pi a^2$ and a are the area and radius of the scintillator, respectively, and L is the distance between the fusion neutron source (i.e., the center of the bubble cluster in the flask) and the scintillation-based detector.

(2) Neutron transport which involves down-scattering energy losses of the neutrons on their way to the scintillator. As a consequence, the initial (from the bubble cluster) monoenergetic (2.5 MeV) D + D fusion neutron flux assumes an energy spectrum from 2.5 MeV to thermal energies, which is characterized by a coefficient ψ_{sh}, i.e. by the time it reaches the scintillator.

(3) Discriminating the scintillations due to neutrons from those due to gammas from the neutron absorption/scattering background. In the first place, pulse shape discrimination (PSD) was applied to reject the dominant gamma photon pulses. Second, the lower-level threshold of the discriminator was set to count only those scintillations corresponding to neutron energies over some minimum threshold energy E_{min}. The discrimination can be ideally characterized by the coefficient φ_d defined as

$$\varphi_d \sim 1 - \frac{E_{min}}{E}\,. \tag{3.2}$$

Consequently, in order to obtain the actual efficiency, one must calibrate the detection efficiency using a pre-calibrated (certified) neutron source. Anyway, without accounting for the loss of efficiency due to PSD, the estimated overall idealized efficiency of the detection system for the D + D fusion neutrons emitted from a bubble cluster in a test chamber filled with chilled D-acetone was calculated by the following formula

$$\eta = \eta_s \varphi_d \psi_{sh} \Omega\,, \tag{3.3}$$

where Ω and φ_d are defined by relations (3.1) and (3.2).

Table 1. Experimental and calculated parameters determining the efficiencies of neutron detection.

η_s	E_{min}	φ_d	ψ_{sh}	Ω	η_2 calculated by Eqn (3.3)	η_2 calibrated by Pu – Be source	References
0.1	0.7	0.7	0.5	0.037	1.3×10^{-3}	0.6×10^{-3}	[10 – 12]
1.0	2.0	0.2	0.25	0.006	0.3×10^{-3}	10^{-5}	[25]

Analysis of the shielding and down-scattering of the emitted 2.5-MeV neutrons in the D-acetone filled test chamber leads to the estimate: $\psi_{sh} \approx 0.5$ [18] (without thermal insulation and without ice packs). To reject the signals of 99% of the gamma ray photons, the lower level of our discriminator was set at $E_{min} = 0.7$ MeV. Thus, the calculated efficiency for our test chamber ($a = 2.5$ cm and $L \approx 6.5$ cm) is $\eta = 1.3 \times 10^{-3} \ll \eta_s = 0.1$ (see Table 1), which is naturally much less than the intrinsic efficiency (η_s) itself. Also, Table 1 gives a summary of the net efficiency of our neutron detector system and that of Shapira et al. [25], which will be discussed subsequently.

In our published studies [10–12], we directly measured the *actual* overall efficiency of our NE-213-based detection system using a NIST-certified 1.0-Ci Pu – Be neutron source emitting $\sim 2 \times 10^6$ n/s (80% of the emitted neutrons had an energy of < 5 MeV), and appropriately corrected for solid angle, PSD, and down-scattering effects for the actual configuration (without thermal insulation and without ice packs). Based on these calibration experiments, the net efficiency for our neutron detector was found to be

$$\sim 0.6 \times 10^{-3} . \tag{3.4}$$

Thus, the *measured* efficiency of our neutron detection system was lower by a factor of ~ 2 than the idealized theoretical value (which did not include PSD-related reduction). Significantly, this value is lower by a factor of ~ 170 than $\eta_s = 0.1$, which was used by Goverdovskii et al. [24] to claim that we had overstated the neutron emission rate in our experiments by almost 10^3 times.

There is one more important fact. The measured and estimated efficiencies η_2 correspond to the detection efficiency for the secondary neutrons emitted from the central zone of the flask. The detection efficiency for the primary neutrons, η_1, is determined by the ratio of the number N_1 of background scintillations for time Δt to the emission of neutrons from the PNG during the same time interval, $Q_1 \Delta t$ (where Q_1 was known from the certificate of PNG or special calibration experiments):

$$\eta_1 = \frac{N_1}{Q_1 \Delta t} . \tag{3.5}$$

Taking into account formulas (2.3) and (2.5), the ratio between the efficiencies of the primary and the secondary neutrons is written out as

$$\frac{\eta_1}{\eta_2} = \frac{Q_2}{\chi Q_1} \quad \text{or} \quad Q_2 = \frac{\eta_1 \chi}{\eta_2} Q_1 . \tag{3.6}$$

For the conditions of our experiments, the detection efficiency η_1 for the primary neutrons was higher than the detection efficiency for the secondary neutrons, η_2, because the primary (14.1 MeV) neutrons do not significantly scatter in the flask, which was filled with D-acetone. In addition, for primary neutrons having energy $E_1 > E_2 = 2.5$ MeV (see the description of the above factor No. 2), the discrimination coefficient φ_d was also higher [see Eqn (3.2)].

To estimate the neutron balance, Goverdovskii et al. [24] mistakenly used underestimated values of η_1 and χ, notably, instead of η_1 they used η_2, and instead of $\chi = 0.04$ for the conditions of our ORNL experiments [10] [see formula (2.5a)], and $\chi = 0.35$ for the conditions of work [11] [see formula (2.5b)], they used $\chi = 0.02$. As a result of these mistakes, the neutron balance in Ref. [24] turned out wrong, which made their criticism of our neutron balance groundless.

Goverdovskii et al. [24] also criticized our estimation of the efficiency of the neutron detection system used by Shapira and Saltmarsh [25], when they placed their plastic detector (see PD scintillator in Fig. 2) alongside, but rather distant from, our experimental apparatus, while *we conducted* two of our many tests at ORNL [their physics detector (PD) system will be denoted herein as ShS]. Their very large PD scintillator had a tenfold greater intrinsic efficiency $\eta_s \approx 1.0$ than ours but a much higher background count rate. One has to draw attention of our critics [24], once again, to the three above-mentioned factors.

(1) The PD scintillator could not fit in the refrigerated box that housed the acoustic chamber, so it was placed relatively far from the test flask having the bubble clusters. As a consequence, the solid angle (3.1) between the PD scintillator and the flask filled with D-acetone was one sixth that of our NE-213 detector (see Table 1).

(2) More than half of the 2.5 MeV neutrons were lost in the plastic walls and thermal shielding of the refrigerated space after leaving the flask but before reaching the PD scintillator, and this contribution to the efficiency was estimated as $\psi_{sh} < 0.5 \times 0.5 = 0.25$.

(3) In the ShS measurement system, a pulse shape discriminator to eliminate the main part of the scintillations due to gamma photons did not work well during the periods of highest count rates. To reduce unwanted background signals, the discrimination level for the ShS system was set at $E_{min} = 2$ MeV, which is very close to the energy of the 2.5-MeV D + D fusion neutrons of interest. Thus, the fraction of counted secondary neutron scintillations was substantially smaller than that for our detector. In fact, because of formula (3.2) it was $\varphi_d < 0.2$.

As a result, according to formula (3.3), the calculated net efficiency of the ShS neutron detection system [25] for the measurements at our setup was almost one fifth that of ours (see Refs [10–12] and Table 1).

Apart from this theoretical estimation, the efficiency of the ShS system used in the measurements at our setup was, like the efficiency of our system, determined with a calibrated Pu – Be neutron source. It was actually less than 1/60 the efficiency of our system (see Table 1), which is apparently attributed to $\psi_{sh} < 0.25$ and $\varphi_d \ll 0.2$, owing to the energy losses for most of the fusion neutrons to values much lower than $E_{min} = 2$ MeV (ShS' setting of their discriminator). As will be discussed subsequently, this conclusion is confirmed by measured and calculated neutron scintillation spectra.

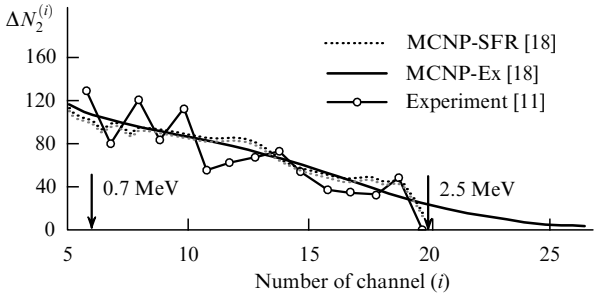

Figure 4. Numerical [18] and measured spectra of secondary neutrons for particular experimental conditions [11].

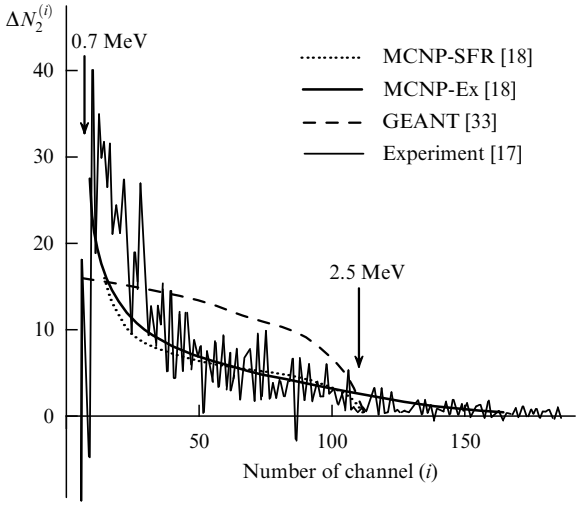

Figure 5. Numerical [18, 33] and measured spectra of secondary neutrons for particular experimental conditions [17].

Nevertheless, Shapira and Saltmarsh [25] did show a statistically significant increase in thermonuclear neutron emission ΔN_2 (i.e., over 7 SD), but because they overestimated the efficiency of their neutron detection system by three orders of magnitude, they incorrectly concluded in their report that the production of D + D fusion neutrons, Q_2, was negligible and also incompatible with our published tritium emission rate [10].

In spite of our criticisms of their ShS detection system analysis, which were presented in various publications [10, 11, 29] and at seminars and conferences where Shapira and Saltmarsh were present, they never answered our arguments, which are obvious to any nuclear measurement professional.

Goverdovskii et al. [24] expressed concerns that for the data measured in Refs [11, 20] "both original and differential spectra produce more skepticism than optimism for confidence concerning the existence of the phenomenon in principle." This criticism is also completely unwarranted. They obviously did not consider our paper [18], where the measured spectrum profiles were compared with experiment-specific predictions from the well-known and widely accepted industry standard neutron transport codes. To explain this, we need to give a brief account of the issue.

In addition to the overall neutron production ΔN_2, we also published in Refs [10–13, 15–20] the measured energy-dependent pulse height amplitudes A (i.e., the amplitude spectra). To determine such distributions, the ranges of scintillation amplitudes for the primary neutrons from the

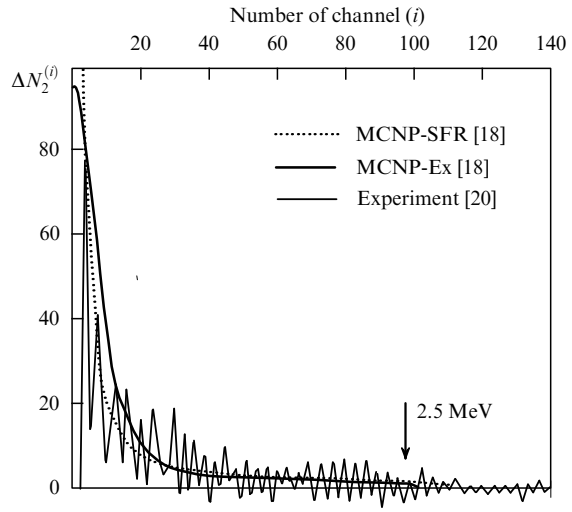

Figure 6. Numerical [18] and measured spectra of secondary neutrons for particular experimental conditions [20].

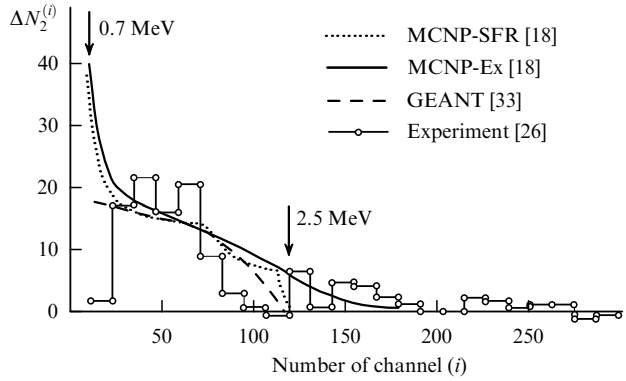

Figure 7. Numerical [18, 33] and measured spectra of secondary neutrons for particular experimental conditions [26].

GPN and the secondary neutrons from the flask were divided into subranges (channels) of value $A^{(i)}$. The range marked as

$$A^{(i-1)} < A < A^{(i+1)} \tag{3.7}$$

is named the ith channel. For each such channel, the number of scintillations $N_1^{(i)}$ without bubble cavitation and the number of scintillations $N_c^{(i)}$ with bubble cluster cavitation were measured. Their difference, namely

$$\Delta N_2^{(i)} = N_c^{(i)} - N_1^{(i)}, \tag{3.8}$$

defines the number of neutron scintillations in the ith channel (i.e., with energies in the range of interest). Finally, for all channels one has

$$\Delta N_2 = \sum_i \Delta N_2^{(i)}. \tag{3.9}$$

The measured scintillation spectra of secondary neutrons produced due to bubble cluster cavitation under different experimental conditions are plotted in Figs 4–7 by thin solid lines.

In 2008, besides the measured spectra, our group published the corresponding calculated neutron spectra for

the above-mentioned experiments [18]. These spectra are shown in Figs 4–7 as solid (thick), dotted, and dashed lines.

Two independent computational methods were utilized as cross-checks on each other. Both methods were based on the well-established MCNP code [29, 30], which used the Monte Carlo N-Particle Transport method. These calculations simulate the scattering process and energy loss of neutrons due to collisions along their trajectories from the place of generation in the center of the flask (where they are monoenergetic with an energy of 2.5 MeV) to the scintillator.

All probable neutron trajectories and their energy losses depend on the equipment surrounding the flask and, particularly, on the NE-213 scintillator. The resulting neutron spectrum at the place of location of the NE-213 liquid scintillation (LS) detector was also modeled for predicting the detector's pulse height and proper spectral response using two independent approaches. In the first, the USDoE-sponsored Scintillation Full Response (SFR) Monte Carlo code [31], which was specifically developed to predict the response of an ideally constructed and setup NE-213 LS detector system, was utilized together with the input neutron spectra predicted by the MCNP code [30]. This approach is referred to as MCNP-SFR in Figs 4–7. The second approach relied on the experimental data of Lee and Lee [32] for the actually measured pulse height spectral data acquired from an NE-213 LS detector for known incident neutron energy and, together with the MCNP code [30], predicted down-scattered neutron spectrum. This independent approach for deriving the expected pulse height neutron spectrum is referred to as MCNP-Ex.

The above experimental data and the Monte Carlo code predictions for the conditions of our experiments [11, 17] and those of other groups [20, 26] are shown in Figs 4–7. Figure 4 pertains to the external PNG neutron-nucleated bubble fusion experimental data taken at Oak Ridge National Laboratory (ORNL) by our group [10, 11]. Figure 5 demonstrates self (alpha-recoil)-nucleated bubble fusion experimental data taken at Purdue University by our group [17]. Figure 6 refers to the external isotopic neutron source-nucleated bubble fusion confirmatory experimental data taken at Purdue University by Xu and Butt [20]. Finally, Figure 7 concerns the self (alpha-recoil)-nucleated bubble fusion confirmatory experimental data taken by Forringer et al. [26].

It is important to recognize that these experimental data were all acquired, analyzed, and published by our group and two other scientific groups without knowledge of the expected (i.e., computer code-predicted) pulse height neutron spectra for the various complex experimental system configurations which were utilized.

Figures 4–7 show that the calculations based on MCNP-SNF and MNCP-Ex codes confirm the production of 2.5-MeV secondary neutrons (in a flask with chilled D-acetone due to cavitation) in the experiments by our group [10, 11, 17] and in several confirmatory experiments [20, 32]. Thereby, the measured and calculated neutron spectra show that the 'skepticism' of Goverdovskii et al. [24] on cavitational production of thermonuclear neutrons is unfounded.

In addition to the skepticism presented in paper [24], a paper by Naranjo [33] was published earlier in 2006. In this paper, a computed neutron spectrum was presented for conditions of our group's experiment [17] when cavitation was initiated by dissolved uranium α-particle recoils. B Naranjo applied the GEANT Monte Carlo code and his calculated spectra are plotted in Fig. 5 (dashed line) and compared with the experimental data [17] of our group, which are shown by the thin broken line. In Naranjo's opinion, the very significant discrepancy between his results and our data was evidence that somewhere near our experimental setup there was a Cf-252 neutron source. He also suggested that this source was used by our group for the purpose of falsification. This slanderous allegation was published by journalist E Reich in *Nature News* [22] without any scientific discussion before publishing Naranjo's paper in *Physics Review Letters*. The resulting scandal forced us to do correct and detailed calculations of the neutron spectra in our own and our colleagues' confirmatory experiments.

The explanation of the discrepancy between Naranjo's calculated spectra and our data [17] turned out to be very simple [18, 19]. In his calculations, Naranjo did not take into account the $\approx$ 3-cm-thick ice (H_2O) packs (shown in Fig. 2 by the double dashed lines), which shielded the scintillator from the test chamber (see the NE-213 scintillator on the right-hand side of the flask in Fig. 2). Correct calculations including the ice packs (see dotted and dark solid lines in Fig. 5) agree well with the experimental data [17] (the thin broken line in Fig. 5), while the GEANT simulations of Naranjo (which did not take into account the ice packs) do not. In contrast, the GEANT (Naranjo) model does properly simulate the confirmation experiments by Forringer et al. [26] (see Fig. 7), in which the thermal insulation did not shield the detector from the test chamber (see the NE-213 scintillator on the left-hand side of the flask in Fig. 2), because their test chamber was mounted in a freezer, and thus ice packs were not needed. As seen in Fig. 7, the calculations with all three codes, including those by the GEANT code (see the dashed line), agree well with each other and with the experimental findings by Forringer et al. [26].

In addition, some earlier critics, and now Goverdovskii et al. [24], claimed that we had not accounted for PNG source neutron absorption by D-atoms in the liquid pool during the production of tritium (T) atoms. Actually, we did indeed account for this effect [11]. However, to do so one must also account for the GPN neutron production rate and the solid angle subtended by the D-acetone in the test chamber from our PNG. In any case, we found in work [11] that the total neutron rate impinging on the D-acetone volume has an upper bound of $\sim 6 \times 10^3$ n/s. Even if we assume each and every neutron was absorbed by D-atoms, this would produce about 10^2 fewer T nuclei per second than the $(4-6) \times 10^5$ T/s which we measured [10–12]. However, if one takes into account the cross sections for neutron absorption by D-atoms (from 1 mb $= 10^{-31}$ m^2 for thermal neutrons to 0.01 mb $= 10^{-33}$ m^2 for 14.1-MeV PNG neutrons), and utilizes the total number of D-atoms in the flask ($\sim 10^{25}$), then this source for T nuclei production rate is less than 1 T atom per second.

Nevertheless, in order to overcome any lingering doubts and to confirm experimentally that D + D fusion was the only credible source of our measured tritium ions following bubble cluster cavitation in chilled D-acetone, seven control experiments were performed. In these experiments, the PNG and AG operated as before for all regimes. Four of these regimes were without cavitation, with both chilled and room temperature D-acetone and H-acetone. The other three involved bubble cluster cavitation: one with room temperature D-acetone, and two with chilled and room temperature H-acetone. All these control experiments gave evidence that

there was no measurable T production by the D + n or any other reaction (e.g., C^{13} + n and Li + n) in the glass flask.

Thus, these experiments clearly showed that the tritium nuclei that were measured could only be produced by the D + D thermonuclear fusion reaction, in which both 2.45-MeV neutrons and tritium ions are produced during bubble cluster cavitation in chilled D-acetone.

4. Theoretical analysis of the supercompression of vapor bubbles

The process of the impact of relatively strong acoustic waves on a bubble cluster leading to the collapse of vapor bubbles within the cluster is a multiscale process with *sharpening* (blow-up). Along the process time and spatial scales, the scales of the physical parameters (velocity, density, pressure, and temperature) change by many orders of magnitude. For example, the time scale changes from 10^{-5} s to 10^{-12} s, and the spatial scale changes from 10^{-2} m to 10^{-8} m. Consequently, the physical mechanisms and governing equations change, too.

In particular, on the bubble cluster's spatial scale (10^{-2} m) compression focusing takes place not in a gas but in a two-phase bubbly liquid. This process is described by continuum mechanics equations [34, 35] with two pressures, where the pressures in the continuous liquid phase and in the gas within the dispersed bubbles are different. This difference in pressure induces a liquid microflow around the bubbles in the bubble cluster, which, in turn, produces changes in the bubbles' size. During this stage, the compressibility of the liquid is negligible, and the microflows are described by the Rayleigh–Plesset equation (see, e.g., book [34]). Numerical solutions of the conservation equations [9] expose a wavy process within the spherical bubble cluster and the inhomogeneous density and pressure of the liquid within the cluster. In response to focusing the spherical wave within the bubble cluster, the pressure of the liquid around the bubbles in the central zone of the bubble cluster grows from 15 bar to ≈ 200 bar during the compression stage, and its characteristic duration falls from $t_p \approx 20$ μs to $t_p \approx 5$ μs [9]. In consequence of this bubble cluster cumulation phenomenon, the pressure around the interior bubbles, which drives bubble compression, turns out to be many times higher than on the periphery of the cluster.

As a result, compression of the vapor in the individual bubbles (from 10^{-3} m to 10^{-4} m in size) takes place as a shockless compression, until a regime with a shock wave is realized at spatial scales of $\sim 10^{-5}$ m near the centers of the bubbles. All these specific features have been analyzed and reported on previously [9, 13–16].

To illustrate the above-mentioned features, several figures are presented for the implosive collapse mode of a vapor bubble in chilled D-acetone and in water (H_2O). They summarize the most salient results that have been previously published [9].

For the calculations of high-pressure physics, the Mie–Grüneizen equation of state [3, 34] was employed. This allows taking into account the internal energy and pressure caused by intermolecular potential forces (i.e., the 'cold energy' and 'cold pressure') in the liquid and strongly compressed vapor phases. During the shock wave stage, compressibility of the liquid phase takes place, as does dissociation and ionization of the vapor during a final stage of the bubble collapse.

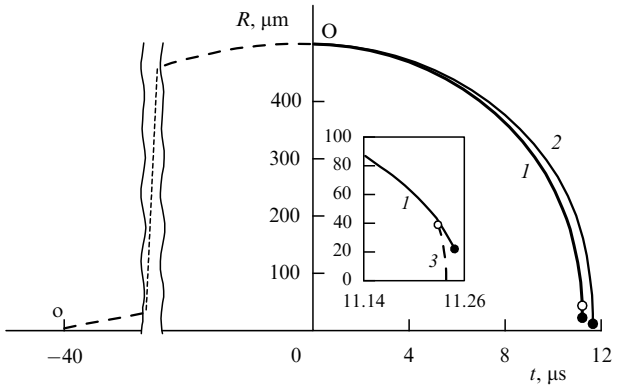

Figure 8. Change in vapor bubble radius $R(t)$ by acoustic impact. The dashed line oO corresponds to the rarefaction stage when the bubble is growing, and lines *1* and *2* correspond to the pressure increase when the bubble is compressing: curve *1* for D-acetone, and curve *2* for water. Moments of minimum radius are marked by black dots, and the moment of the shock wave formation is marked by a white dot. In the insert, a scaled up segment of line *1* is shown together with dotted line *3* corresponding to the collapse of the shock wave converging to the center of the bubble.

Figure 8 illustrates the evolution of the bubble radius R with time t in water and in D-acetone under an acoustic pressure field focused on the center of a bubble cluster. The dashed line oO corresponds to the expansion stage of a cavitated bubble during rarefaction of the pressure field, when the bubble grows during ~ 40 μs from $R \approx 0$ to $R = R_0 = 500$ μm. The solid lines correspond to the compression stage, when during a short time (i.e., 11.2 μs) the bubble radius decreases from $R = R_0 = 500$ μm to a minimum size of $R_{\min} \approx 23$ μm for D-acetone (line *1*), and $R_{\min} \approx 11$ μm for water (line *2*). The moments ($t = t_{\min}$) when the radius of the bubble reaches its minimum size are marked by black dots.

Figure 9 displays the corresponding distributions of pressure $p(r)$, density $\rho(r)$, and temperature $T(r)$ in the vapor and liquid (i.e., D-acetone and water) for a few instants of time t (curves *1–5* in Fig. 9), during the stage when the interface velocity reaches a high value ($\dot{R} \sim 10^3$ m s^{-1}), and the bubble size is $R < 60$ μm. This figure corresponds to a spatial scale of 10^{-5} m, and a time scale of 10^{-8} s.

Figure 10 depicts the change in the D-acetone vapor density near the center of a collapsed bubble ($r = r_{**} = 25$ nm, where, as is shown below, the thermonuclear transformation intensity is maximum) on a microsecond scale (left panel) and a picosecond scale (right panel).

The most important features of the implosive collapse of cavitation vapor bubbles are the following. First, much of the compression (from $R = 600$ μm to 250 μm) takes place with a relatively small velocity $|\dot{R}|$ compared to the speed of sound in the vapor, c_s (i.e., $|\dot{R}| < 50$ m s^{-1} for $t < 8$ μs). However, closer to the end of compression, $|\dot{R}|$ grows rapidly to 1300 m s^{-1}, and then decreases even more rapidly to $|\dot{R}| = 0$, when $R = R_{\min} = R_c$.

Second, even if such a shock wave arises in an imploding bubble, it is not formed near the start of bubble compression but closer to the end of the compression process. Thus, when the velocity of the bubble's interface ($|\dot{R}|$) is small compared to the speed of sound in the vapor, c_s (i.e., $|\dot{R}| \ll c_s$), the compression of the vapor initially proceeds in a homobaric (i.e., quasistatic) process, when the pressure and density in the bubble are essentially homogeneous, and grows with time as

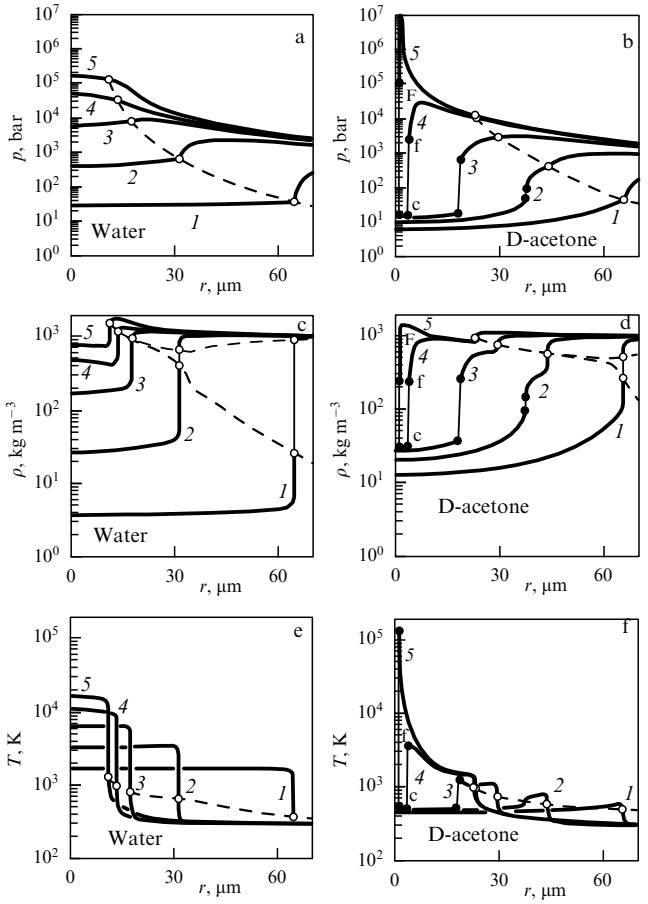

Figure 9. Spatial distributions of vapor pressure (a, b), density (c, d), and temperature (e, f) along radius r during the collapse of a vapor bubble in water (a, c, e) and D-acetone (b, d, f) at five consecutive instants of time (lines *1*–*5*). The white dots correspond to the values of pressure, density, and temperature at the interface of the bubble, and the thin straight-line segments (in figures b, d, f) with black dots correspond to jumps on the collapsing shock wave (e.g., in line *4* this segment is marked cf).

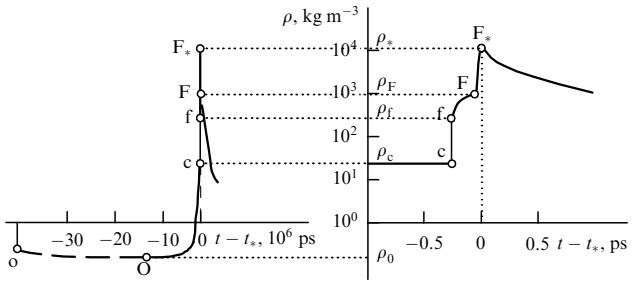

Figure 10. Change in vapor density near the center of an imploding bubble ($r = r_{**} = 25$ nm) of D-acetone vapor on microsecond (left part of figure) and picosecond (right part) time scales. Here, t_* is the instant of time when the radius $r = r_{**}$ and the density reaches the maximum value: $\rho = \rho_{\max} = \rho_*$. The dashed line oO corresponds to the expansion phase of the cavitation bubble (see also the dashed line oO in Fig. 8); the solid line OcfFF$_*$ traces the collapse stage. The solid line Oc illustrates a shockless compression; the thin straight-line segment cf indicates shock-induced compression by a convergent shock wave; fF shows the effect of the continuous compression wave following after the spherical shock wave. And finally, line FF$_*$ corresponds to compression in a divergent shock wave structure, initiated after the reflection of the convergent shock wave structure cfF from the center of the bubble [9].

the bubble is compressed [9]. Later on, as the velocity $|\dot{R}|$ grows sufficiently large, a compression wave arises, which can transform to a shock wave at a distance Δr from the interface $r = R$:

$$\Delta r \sim \frac{c_s^2}{|\ddot{R}|}\,, \qquad |\ddot{R}| \sim \frac{\Delta p}{\rho_L |\dot{R}|}\,, \tag{4.1}$$

where $\ddot{R}$ is the acceleration of the interface, Δp is the pressure difference between the liquid and vapor, and ρ_L is the density of the liquid. The speed of sound in vapor, c_s, as long as its density is much smaller than density of the liquid ($\rho \ll \rho_L$), is given by

$$c_s^2 = \gamma \frac{\mathcal{R}}{M}\, T\,, \tag{4.2}$$

where $\mathcal{R} = 8314\ \mathrm{m^2\ s^{-2}\ K^{-1}}$ is the molar gas constant, and M and γ are the molecular weight and adiabatic exponent of the vapor, respectively. For D-acetone, $M = 64$, $\gamma = 1.125$, while for water vapor $M = 18$, and $\gamma = 1.3$.

For our conditions of interest, $T_0 \approx 273 - 290$ K, $\Delta p \sim 10^2$ bar, and small bubbles (i.e., $R \sim 0.5$ mm) filled with water vapor ($\Delta r \sim 1$ mm $> R$) are considered. That is, the inward distance from the bubble interface to the place where a shock could be formed is in fact larger than the bubble's radius; thus, no shock wave can be formed in an imploding bubble filled with a water vapor. Rather, the compression proceeds with a pressure distribution close to homogeneous, practically without focusing, which is limited by the acoustic generator's (AG) power, and thermonuclear conditions cannot be reached. This is fully supported by our experiments. Indeed, all endeavors to produce D + D fusion neutrons and tritium when using heavy water (D_2O) in our experimental setup [10] turned out to be ineffective, because there was no shock wave focusing within the imploding bubbles

In contrast, in D-acetone vapor bubbles, in which the square of the sound speed, c_s^2, is 3.5 times smaller than in water vapor, $\Delta r \sim 0.2$ mm $< R$, which obviously is less than the bubble's radius, and thus the formation of a shock wave is physically possible. Even so, a shock wave is only formed after significant compression of the bubble from $R_0 = 500$ μm to $R \approx 45$ μm and at a radius of $r_{f0} \approx 40$ μm. This moment is marked in Fig. 8 by the white dot in line *1*, corresponding to D-acetone, and the pressure, density, and temperature distributions at this moment are shown by lines *2* in Fig. 9b, d, f. The convergence of the shock wave to the bubble's center, $r_f(t)$, is illustrated by dashed line *3* in the insert to Fig. 8.

Thus, during the whole time of bubble compression from $R_0 = 500$ μm to $R_{\min} = 23$ μm, the compression from an initial radius of $R_0 = 500$ μm to $R = 45$ μm occurs in a shockless regime. Moreover, the duration of the shock wave stage is only $\sim 10^{-9}$ s in duration out of the total time of bubble compression of $\sim 10^{-5}$ s.

It is important to keep in mind that a convergent shock wave cf (formed at $r_{f0} \approx 40$ μm) propagates through the shocklessly compressed vapor (see Oc in Fig. 10) (at point c: $p_c \approx 15$ bar, $T_c \approx 500$ K, and $\rho_c \approx 27$ kg m^{-3}). This shock wave is focused on the center of the bubble, which leads to a significant cumulative effect in the central part of the imploding vapor bubble. Indeed, it is this wave structure (cfF in Figs 9 and 10) that is focused on the central zone of bubble. This focusing leads to extreme concentration of

kinetic energy and its transformation into the internal energy of a highly compressed substance, thus ending the bubble compression.

On approaching the center of the bubble, the shock wave becomes strong when the pressure after the shock wave (i.e., the jump) exceeds by many times the pressure before the shock wave (see lines *3* and *4* in Fig. 9b, d, f):

$$p_{\mathrm{f}} \gg p_{\mathrm{c}} \,. \tag{4.3}$$

If the density of vapor is not too large ($\rho \ll \rho_{\mathrm{L}}$), and the ideal gas equation of state holds true ($p_{\mathrm{f}} = \rho_{\mathrm{f}}(\mathcal{R}/M)T_{\mathrm{f}}$), then the density of the gas (D-acetone vapor, $\gamma = 1.125$) increases in a jump by a factor [3]

$$\frac{\rho_{\mathrm{f}}}{\rho_{\mathrm{c}}} = \frac{\gamma+1}{\gamma-1} = 17 \,. \tag{4.4}$$

Taking into account that $\rho_{\mathrm{c}} \approx 20\ \mathrm{kg\,m^{-3}}$ and that for high density the 'cold' pressure of intermolecular interaction yields $\rho_{\mathrm{f}} < 20 \times 17 = 340\ \mathrm{kg\,m^{-3}}$, it is actually $\rho_{\mathrm{f}} \approx 250\ \mathrm{kg\,m^{-3}}$.

After converging to the center of the bubble, the spherical shock wave (cf) is followed by a continuous compression wave (see fF in Fig. 10). The effect of this wave consists in increasing the vapor density by 3–4 times. At the moment when the radius of the shock wave is $r_{\mathrm{f}} \approx 1\ \mu\mathrm{m}$, the density after the wave fF is $\rho_{\mathrm{F}} \approx 10^3\ \mathrm{kg\,m^{-3}}$, and the temperature is $T_{\mathrm{F}} \approx 10^5\ \mathrm{K}$. However, even these parameters are far from the maximum which actually occurs, and not enough for significant D + D fusion to occur.

Maximum values of the density and temperatures are achieved during the process of reflection of the convergent wave structure cfF from the center of the bubble and the formation of a divergent multiwave structure FF_* (see Fig. 10). In this multiwave structure, the gas is compressed ~ 10 times more. The process has scales of 10^{-7} m and 10^{-12} s. Our calculations [9] have shown that during this process the gas is dissociated and fully ionized, having the form of plasma which consists of the deuterium, carbon, and oxygen nuclei and electrons. Consequently, a zone of hot plasma with radius $r_* \sim 10^2$ nm is formed, where the density and temperature are $\rho_* \sim 10^4\ \mathrm{kg\ m^{-3}}$ and $T_* \sim 10^8\ \mathrm{K}$ during a time interval of 10^{-12} s. That is clearly the zone where sharpening (or *blow-up*) takes place.

In this zone, there are about 2×10^9 nuclei with a mean internuclear distance of $l_{\mathrm{n}} \sim 10^{-1}$ nm. The Knudsen number for this zone is $\mathrm{Kn} = l_{\mathrm{fp}}/r_* \sim 10^{-2}$, where l_{fp} is the ion mean free path [9]. Therefore, this zone may be analyzed using a continuum mechanics approximation with shock waves, together with a two temperature thermodynamic approximation, since the temperatures of the ions T^{i} and electrons T^{e} are different.

Let us next consider the production of fusion neutrons and tritium nuclei due to energetic binary collisions between deuterium (D) nuclei (the number of collisions being proportional to ρ^2) in the hot plasma zone. Fusion neutron production is defined by a convolution integral [9]:

$$N(t,r) = \int_0^R N_r(t,r)\,\mathrm{d}r \,, \quad N_r(t,r) = \int_0^t f\left(T^{\mathrm{i}}(t',r)\right)\rho^2(t',r)\,\mathrm{d}t' \,. \tag{4.5}$$

The function $f\left(T^{\mathrm{i}}\right)\rho^2$ is determined by D + D fusion reaction kinetics [36], which are dependent on the deuterium ion temperature T^{i}.[4] A careful analysis [9] shows that the passage to the limits yields for D + D thermonuclear kinetics:

$$N_r(r) \underset{r\to 0}{\to} 0 \,, \qquad N_r(r) \underset{r\to\infty}{\to} 0 \,. \tag{4.6}$$

The first asymptotic occurs even for dissipation-free media (for instance, for the Guderley solution), even though

$$T^{\mathrm{i}} \underset{r\to 0}{\to} \infty \,, \qquad f(T^{\mathrm{i}}) \underset{r\to 0}{\to} \infty \,. \tag{4.7}$$

The point is that as $r \to 0$ the time $\Delta t_*(r)$ at the extreme temperature tends to zero:

$$\Delta t_*(r) \underset{r\to 0}{\to} 0 \,. \tag{4.8}$$

For the regimes considered and D + D reaction kinetics, $N_r(r)$ reaches a maximum at $r_{**} \approx 25$ nm. In contrast, for $r < r^\circ \approx 5$ nm and $r > r_* \approx 100$ nm, the kernel function $N_r(r)$ is very small and does not significantly contribute to the integral that determines fusion neutron production N. Thus, the details of the complicated shock wave process in the zone $r < r^\circ \approx 5$ nm are not substantial, because, although the extreme density and temperature are higher in this zone than at $r = r_* \approx 25$ nm, the time interval for the deuterium nuclei at these parameters is much less [see formula (4.8)]. Therefore, the contribution from the zone $r < r^\circ \approx 5$ nm to the D + D reaction can be neglected.[5]

Hydrocode type calculations [9] have shown that in our bubble fusion experiments [10, 11, 17, 20] for each collapse of a cavitation vapor bubble in the extreme zone, $r < r_* \sim 100$ nm, one expects $N_* \sim 10$ thermonuclear neutrons per energetically imploded bubble during its existence time $t_* \sim 10^{-12}$ s, and the same number of tritium nuclei [9].

As noted previously, periodic bubble cluster cavitation occurred in our bubble fusion experiments. In this regime, the extreme cluster collapse of bubbles took place periodically at a frequency of f_2 [see formula (2.1)]. If in this regime $n_* \sim 10$ bubbles in the central zone of the bubble cluster are energetically imploded such that they undergo thermonuclear fusion [9], we arrive at the following productivity of tritium nuclei and 2.5-MeV neutrons:

$$Q_2 = f_2 n_* N_* \sim 10^5\ \mathrm{n/s} \,. \tag{4.9}$$

This agrees quite well with our experiments [10–12] [see Q_2 in formula (2.1)].

The influence of dissociation, ionization, and radiation and the corresponding energy losses which could reduce the ion temperature T^{i} have also been carefully considered [9]. Significantly, during the time interval of $t_* \sim 10^{-12}$ s, when a

[4] The dependence considered of kinetics on the ion temperature [36] is for a deuterium plasma with a ratio between numbers of electrons and deuterium nuclei equal to 1 : 1. But for plasma formed by D-acetone vapor, besides deuterium, one also faces carbon and hydrogen nuclei. In an entirely ionized plasma, there are 4 excess electrons for each deuterium nucleus. That is, four electrons are produced per one deuterium nucleus. This excess can lower the Coulomb barrier for deuterium nuclei interactions when the density of the plasma is high enough and can lead to much higher thermonuclear reaction rates. This consideration was previously suggested by A A Rukhadze and V A Simonenko.

[5] The N value calculated by the convolution integral (4.5) can be considered as a quantitative characteristic of the efficiency of the particular regime of cumulation for realization of physico-chemical transformations with proper kinetics.

fusion parameter zone is formed and gas dissociation and ionization occur, the electron temperature does not have sufficient time to noticeably approach the temperature of the ions. That is, the inequality

$$T^{\mathrm{e}} \ll T^{\mathrm{i}} \tag{4.10}$$

is satisfied.

This ensures low energy losses due to the heating of electrons and their radiation losses, and thus a low influence of these losses on thermonuclear productivity Q_2.

Finally, we note that the formation of vapor/plasma bubbles in a liquid by powerful laser pulses does not look promising for ultracompression due to two reasons. First, after the focused laser-induced 'explosion' in the liquid the mass of the gas is too large to be compressed by the acoustic field. Second, dissociation of the vapor immediately occurs after the laser 'explosion'. This increases the speed of sound in the gas/plasma dramatically and thus decreases shock wave cumulation.

5. Analysis of some critical remarks on the theory

The process of D-acetone vapor bubble collapse from an initial radius of $R_0 = 500$ μm to a minimum radius of $R_{\min} \approx 23$ μm passes through different scales with a distinct physical content, namely:

1) wave compression and focusing in the bubble cluster ($r_{\mathrm{cl}} \approx 1$ cm);

2) shockless compression of vapor in the bubbles when their radius decreases from $R_0 = 500$ μm to $R \approx 45$ μm in $t_{\mathrm{c}} \approx 10^{-5}$ s;

3) shock wave structure formation at $r_{\mathrm{f0}} \approx 40$ μm and its converging to the center of the bubble in $t_{\mathrm{s}} \approx 10^{-9}$ s;

4) reflection of this shock wave structure from the center of the bubble with the formation of a 'nano/pico' thermonuclear zone ($r_* \sim 10^2$ nm, $\Delta t_* \sim 10^{-12}$ s) where, due to all four of these stages, the vapor density increases from $\rho_0 \approx 0.25$ kg m^{-3} to $\rho_* \sim 10^4$ kg m^{-3}.

In contrast, in the paper by Goverdovskii, Imshennik, and Smirnov [24], all this multiscale process is described by a model describing one physical process — the convergence of a spherical shock wave to the center in vapor according to the well-known Guderley's self-similar solution for a gas with an adiabatic exponent $\gamma = 5/3$. The initial density of vapor was assumed to be $\rho_{\mathrm{c}} = \rho_0 = 10$ kg m^{-3} (but this value of density is unsubstantiated), and it was assumed that a shock wave is formed at $r_{\mathrm{f0}} = 1$ cm. This value is not substantiated, either. Following the power law in Guderley's solution, Goverdovskii et al. [24] then calculated that the temperature reaches a 'thermonuclear' value, $T_{\mathrm{f}}^{\mathrm{TF}} > 3 \times 10^6$ K (why this temperature is supposed to be thermonuclear is unsubstantiated; however, the time of stay is important, too) in a sphere of radius $r_{\mathrm{f}}^{\mathrm{TF}} = 0.4$ μm. In their model, this zone contains 10^7 nuclei (for $r_{\mathrm{f}} = 40$ kg m^{-3}), with an energy of 0.3 keV, even if $\rho_0 = 10$ kg m^{-3}. It is certainly true that for these parameters one would not expect any thermonuclear neutrons. Moreover, an arbitrary assumed value of the initial radius of the shock wave $r_{\mathrm{f0}} = 1$ cm is 25,000 times as great as the shock wave radius $r_{\mathrm{f}}^{\mathrm{TF}} = 0.4$ μm, at which, by their estimation, the thermonuclear temperature can be reached. This is the basis for the authors of paper [24] to state the unreality of such spherically symmetric cumulation, as the shock wave radius should decrease 25,000-fold. Clearly such a model is not realistic.

In any case, without arguing about the suitability of Guderley's solution and the unreality of spherically symmetric cumulation, it has been known for a long time that one shock wave cannot produce sufficient compression for the realization of thermonuclear reactions, since one shock wave compression (i.e., density increase) is limited by formula (4.4). For the accepted value of adiabatic exponent $\gamma = 5/3$, it is obtained from formula (4.4) that shock wave compression can increase the density only fourfold (i.e., $\rho_{\mathrm{f}} = 4\rho_0$). Moreover, as noted previously, the primitive scheme based on a Guderley type implosion only is far from the multiscale process which actually occurs in imploding vapor bubbles.

What previously described principal features of a collapsing vapor bubble did Goverdovskii et al. miss?

First, the adiabatic exponent of D-acetone vapor is $\gamma = 1.125$, not 5/3, as assumed by Goverdovskii et al. [24]. The value of $\gamma = 5/3$ occurs only after full dissociation of the C_3D_6O molecules into their corresponding 10 atoms (i.e., in a relaxation time of 10^{-8} s after shock compression [9]). Therefore, an increase in vapor density, $\rho_{\mathrm{f}}/\rho_{\mathrm{c}}$, due to a strong shock wave is, according to formula (4.4), limited by 17, not 4. But this is not the most important thing.

Second, the compression of the vapor before shock wave reflection from the bubble center occurs not only due to the convergent shock wave but at first shocklessly (see the line fragment Oc in Fig. 10), then by shock 'jump' (cf in Fig. 10), and again shocklessly (fF in Fig. 10). As a result, the density of the vapor reaches at least the value of $\rho_{\mathrm{F}} \approx 1000$ kg m^{-3}.

Third, as discussed previously above, maximum values of the density and temperature are reached as a result of reflection of the convergent wave structure cfF from the bubble center and the formation of a plasma nanozone (radius $r_* \sim 100$ nm). In this zone, the plasma has density $\rho_* \approx 10^4$ kg m^{-3} and temperature $T_* \approx 10^8$ K during the time interval $\Delta t_* \sim 10^{-12}$ s. Contrary to our critics' estimations [24], in this zone, in spite of its actual (small) size, there are not 10^7 nuclei, but rather 2×10^9 and the temperature is not about 3×10^6 K, but about 10^8 K.

As was shown above, it is this zone with extreme parameters where the thermonuclear reaction occurs.

Anyway, all these specific features were previously discussed in detail in the open literature [9, 12–16, 19], but they were apparently not taken into account by our critics.

Finally, one of the main obstacles to the formation of nanofusion zones lies in the effect of distortions of spherical symmetry during the shock wave cumulative process. We have also considered this important issue, and have recently published a detailed theoretical investigation based on two- and three-dimensional analyses [37].

This investigation showed that, in spite of developing interfacial instabilities during spherically symmetric cumulation leading to the growth of the symmetry's perturbations, near-spherically symmetric supercompression of *small* vapor bubbles filled with vapor having a *high enough molecular weight* (i.e., low speed of sound) has essential resources for energy cumulation due to the *viscosity* of the liquid, the *high vapor density* close to the bubble's interface, and the *surface tension* at the interface. In fact, surface tension minimizes any initial nonspherical perturbations prior to the onset of the bubble compression process.

We have made numerical calculations taking into account nonspherical microshock waves in the bubble during com-

pression. These calculations showed that, for a well-organized acoustical pressure field, only about 50% of the D + D neutrons and tritium ions might be lost because of nonspherical effects.[6] Nevertheless, this investigation needs more detailed analysis and will be published separately.

The formation of the extreme microzones ~ 10 nm in size is not excluded, even after fragmentation of bubbles in the center of the cluster.

6. Conclusion

Certainly, our small-scale desk-top experiments involving only the acoustic forcing of the cavitation of vapor bubbles and their implosive collapse within the resulting bubble clusters have not produced a fusion burn, but only thermonuclear 'sparks'. Indeed, the experimental setup which we used cannot be considered as a thermonuclear reactor, which could produce net energy [16]. First, in our process, which has a relatively weak neutron productivity, the fusion energy release by thermonuclear sparks is around 10^6 times the energy needed (by the GPN and AG) for initiation of fusion sparks, and this fusion energy does not exert influence on the state of this nanothermonuclear zone. Second, the process occurs at low liquid temperatures (0 °C) only, and thus the energy releases are of low thermodynamic value.

Nevertheless, about two orders of magnitude in the fusion energy release would be gained by using the D + T reaction instead; for example, instead of just using D-acetone as the test fluid, using a mixture of D-acetone and T-acetone (C_3T_6O) with mass concentration ratio $M(C_3D_6O):M(C_3T_6O) = 64:70$. In the search for the other four orders of magnitude needed to break even, the following areas appear to be promising for creating more complete fusion burns, rather than just sparks.

(1) Use of a larger and more robust test chamber design. Our initial test apparatus was a 600-cm^3 volume Pyrex glass test chamber, with a 40-W acoustical generator (AG) coupled to a PZT and a commercially available pulsed neutron generator (PNG).

(2) Use of an optimized test liquid with a higher molecular weight and a larger content of D and T atoms, which would make the first, shockless, stage of vapor compression more effective, so that supercompression could occur at higher pool temperatures (> 100 °C).

Goverdovskii, Imshennik, and Smirnov [24] also wrote about the prospects of traditional fusion programs for the second part of the 21st century. These programs are Tokamak programs [International Thermonuclear Experimental Reactor (ITER) and the Demonstration Power Plant (DEMO)], and laser inertial confinement fusion programs. They lament the long period of waiting for results and question whether they (the 'leading fusion experts') are in the right path. In addition, however, they also claim that 'poorly educated inventors and world-renowned scientists' come in large numbers with 'simple' recipes, and 'leading fusion experts' have had to waste time analyzing these recipes. We note that at least some of the 'leading fusion experts' have been considering these new ideas and prospects not in scientific circles, but in the media and with government officials when protecting the financing of their own research programs. This does not favor the maintenance of a high scientific level by some 'leading fusion experts' or an optimization of fusion research study funding. In any event, the 'leading fusion experts' need to make their criticisms of the recipes of 'poorly educated inventors and world-renowned scientists' at a much higher scientific level.

Many scientists and practising nuclear engineers believe that the expensive and decades-long research programs based on tokamak and laser inertial-confinement fusion concepts are not very likely to result in near-term industrial-scale fusion energy production. In contrast, bubbly liquids open new avenues for use in *industrial power systems*, because the near spherical focusing of energy by a dense (inertial) and viscous liquid is inherently much more stable than the focusing of energy due to a vapor explosion initiated by an optical supershort laser shock. In addition, power supply by supershort laser shocks requires great amounts of energy and giant apparatuses, and it is not effective for the supercompression of a gas.

Fortunately, bubbly liquids show potential in the search for nuclear fusion energy technology, which even our critics [24] admit.

[6] This sentence was added in the English proof.

References

1. Zababakhin E, Zababakhin I *Unlimited Cumulation Phenomena* (Moscow: Nauka Publ., 1990); Translated from Russian: Zababakhin E I, Zababakhin I E *Yavleniya Neogranichennoi Kumulyatsii* (Moscow: Nauka, 1988)
2. Zababakhin E I *Some Problems of the Gasdynamics of Explosions* (Snezhinsk: RFNC — VNIITF Publ. House, 2001)
3. Zel'dovich Ya B, Raizer Yu P *Physics of Shock Waves and High-Temperature Hydrodynamic Phenomena* (New York: Academic Press, 1966–1967); Translated from Russian: *Fizika Udarnykh Voln i Vysokotemperaturnykh Gidrodinamicheskikh Yavlenii* (Moscow: Fizmatlit, 2008)
4. Crum L A, Matula T J *Science* **276** 1348 (1997)
5. Margulis M A *Phys. Usp.* **43** 259 (2000); *Usp. Fiz. Nauk* **170** 263 (2000)
6. Young F R *Sonoluminescence* (Boca Raton: CRC Press, 2005)
7. Moss W C et al. *Phys. Lett. A* **211** 69 (1996)
8. Nigmatulin R I et al. *Sonochemistry and Sonoluminescence* (NATO ASI Ser., Ser. C, Vol. 524, Eds L A Crum et al.) (Dordrecht: Kluwer Acad. Publ., 1999)
9. Nigmatulin R I et al. *Phys. Fluids* **17** 107106 (2005)
10. Taleyarkhan R P et al. *Science* **295** 1868 (2002)
11. Taleyarkhan R P et al. *Phys. Rev. E* **69** 036109 (2004)
12. Nigmatulin R I et al. *J. Power Energy* **218** 345 (2004)
13. Nigmatulin R I et al. *Vestn. Akad. Nauk Resp. Bashkortostan* **7** (4) (2002)
14. Nigmatulin R *Nucl. Eng. Design* **235** 1079 (2005)
15. Taleyarkhan R P, Lahey R T, Jr., Nigmatulin R I *Multiphase Sci. Technol.* **17** 191 (2005)
16. Lahey R T, Jr. et al. *Adv. Heat Transfer* **39** 1 (2006)
17. Taleyarkhan R P et al. *Phys. Rev. Lett.* **96** 034301 (2006)
18. Taleyarkhan R P et al. *Nucl. Eng. Design* **238** 2779 (2008)
19. Taleyarkhan R P, Lahey R T, Jr., Nigmatulin R I, in *Nuclear Energy Encyclopedia*: *Science, Technology, and Applications* (S B Krivit, J H Lehr, T B Kingery) (Hoboken, N.J.: Wiley, 2011) Ch. 46, p. 553
20. Xu Y, Butt A *Nucl. Eng. Design* **235** 1317 (2005)
21. Kennedy D *Science* **295** 1793 (2002)
22. Reich E S *Nature News* March 8 (2006) doi:10.1038/news060306-2; *Nature News* July 22 (2008) doi:10.1038/454379a; *Nature News* August 29 (2008) doi:10.1038/news.2008.1069
23. Krivit S *New Energy Times* July 18 (2013); *New Energy Times* Jan. 20 (2014); http://www.bubblegate.com
24. Goverdovskii A A, Imshennik V S, Smirnov V P *Phys. Usp.* **56** 423 (2013); *Usp. Fiz. Nauk* **183** 445 (2013)
25. Shapira D, Saltmarsh M *Phys. Rev. Lett.* **89** 104302 (2002)
26. Forringer E R, Robbins D, Martin J *Trans. Am. Nucl. Soc.* **95** 736 (2006)

27. Abramov A I, Kazanskii Yu A, Matusevich E S *Osnovy Eksperimental'nykh Metodov Yadernoi Fiziki* (Fundamentals of Experimental Nuclear Physics Methods) (Moscow: Energoatomizdat, 1985)
28. Knoll G F *Radiation Detection and Measurement* (New York: Wiley, 1989)
29. Taleyarkhan R P et al., arXiv:1307.3217
30. X-5 Monte Carlo Team "MCNP" LANL-UR-03-1987 (2003)
31. Dickens J K, "SCINFUL", ORNL-6462 (1988)
32. Lee J H, Lee C S *Nucl. Instrum. Meth. Phys. Res. A* **402** 147 (1998)
33. Naranjo B *Phys. Rev. Lett.* **97** 149403 (2006)
34. Nigmatulin R I *Dynamics of Multiphase Media* Vol. 1 (New York: Hemisphere Publ. Corp., 1991); Translated from Russian: *Dinamika Mnogofaznykh Sred* Vol. 1 (Moscow: Nauka, 1987)
35. Kedrinskii V K *Hydrodynamics of Explosions*: *Experiment and Models* (Berlin: Springer, 2005); Translated from Russian: *Gidrodinamika Vzryva*: *Eksperiment i Modeli* (Novosibirsk: Izd. SO RAN, 2000)
36. Bosch H-S, Hale G M *Nucl. Fusion* **32** 611 (1992)
37. Nigmatulin R I et al. *J. Appl. Mech. Tech. Phys.* **55** 444 (2014); *Priklad. Mekh. Tekh. Fiz.* **55** (3) 82 (2014)